

Spatial von-Mises Fisher Regression for Directional Data

Zhou Lan*

Brigham and Women's Hospital, Harvard Medical School
and

Arkaprava Roy*

Department of Biostatistics, University of Florida
and

for the Alzheimer's Disease Neuroimaging Initiative

June 19, 2024

Abstract

Spatially varying directional data are routinely observed in several modern applications such as meteorology, biology, geophysics, and engineering, etc. However, only a few approaches are available for covariate-dependent statistical analysis for such data. To address this gap, we propose a novel generalized linear model to analyze such that using a von Mises Fisher (vMF) distributed error structure. Using a novel link function that relies on the transformation between Cartesian and spherical coordinates, we regress the vMF-distributed directional data on the external covariates. This regression model enables us to quantify the impact of external factors on the observed directional data. Furthermore, we impose the spatial dependence using an autoregressive model, appropriately accounting for the directional dependence in the outcome. This novel specification renders computational efficiency and flexibility. In addition, a comprehensive Bayesian inferential toolbox is thoroughly developed and applied to our analysis. Subsequently, employing our regression model to the Alzheimer's Disease Neuroimaging Initiative (ADNI) data, we gain new insights into the relationship between cognitive impairment and the orientations of brain fibers along with examining empirical efficacy through simulation experiments.

Keywords: Bayesian Angular Inference, Diffusion tensor imaging, Markov chain Monte Carlo, Tangent-normal decomposition

*

1 Introduction

Directional statistics, alternatively referred to as circular or angular statistics in two-dimensional cases or spherical statistics for higher dimensions, is a distinct subfield of multivariate statistics specifically tailored for analyzing directional data (Mardia and Jupp, 2009). Such data arise when measurements are expressed as angles or directions, inherently exhibiting spherical relationships. Instances of directional data can be found in diverse disciplines, including meteorology, biology, geophysics, and engineering, with examples ranging from wind direction and animal migration patterns to diffusion tensor imaging. Moreover, a variety of external features often exist that control the directional outcome.

In this paper, our proposed methodological developments focus on studying the association between the white matter fiber orientations in the brain, and subject-level covariates (e.g., age, gender, cognitive score, and genetic information), revealing the factors driving the fiber orientations (Schwartzman et al., 2005, 2008). In brain neuroimaging analyses, spatial dependencies become an important feature. Furthermore, the incorporation of spatial dependence is appealing in many directional data applications such as wind direction modeling (Neto et al., 2014; Murphy et al., 2022), brain fiber orientation modeling (Goodlett et al., 2009; Zhu et al., 2011), and modeling actigraph data from wearable devices (Banerjee et al., 2023). Hence, to effectively analyze this type of data, it is important to employ a strategy that can address: a) the inherent directional nature of the outcome; b) the complex spatial dependencies; and c) an effective and convenient summarization tool for the effects of the external factors associated with the outcome.

The fiber orientation data considered in this paper are derived from diffusion tensor imaging (DTI), a technique that has gained wide popularity for its increasing efficiency and accuracy in measuring microstructures (Soares et al., 2013). In the DTI imaging technique, a diffusion ellipsoid, which represents diffusivity in each voxel, is commonly

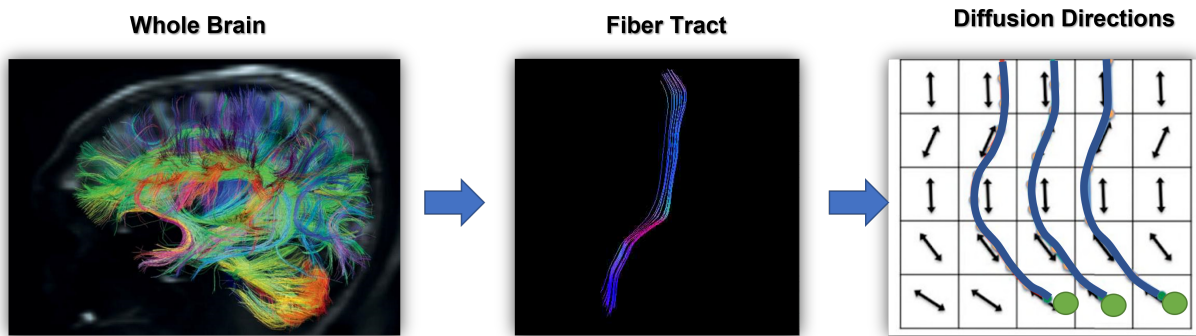


Figure 1: Macro to micro-view of the brain’s anatomical structure: the left panel shows that the brain is connected through the streamlines of fiber tracts; the middle panel provides an example fiber tract; finally, the right panel shows the directional data characterizing the streamlines.

used. Here, we focus on the principal eigenvector \mathbf{E}_1 , interpreted as the tangent direction along the fiber bundle (rightmost panel in Figure 1). Thus, it is referred to as the *principal diffusion direction* throughout the rest of the paper and is one of the most critical markers for studying white matter fibers. The association between principal diffusion directions and subjects’ covariates has emerged as a perspective in studying neurodegenerative diseases (Schwartzman et al., 2005, 2008). With studies revealed that tissue properties may vary systematically along each tract, i.e., tract profiles of white matter properties (Yeatman et al., 2012), it becomes an important scientific question in investigating how the principal diffusion directions along each tract are driven by covariate effects.

Traditional statistical methods, which rely on Euclidean space, are generally unsuitable for analyzing directional data due to their inability to account for the spherical relationships among values. To tackle these issues, directional statistics utilize a unique set of techniques (Gould, 1969) and probability distributions (Johnson and Wehrly, 1978). Several regression approaches have been developed for handling circular or 2-dimensional directional outcome data (Gould, 1969; Johnson and Wehrly, 1978; Fisher and Lee, 1992; Presnell et al., 1998).

However, these approaches are not generalizable for spherical outcomes where the data sits on three or higher-dimensional spheres (Mardia and Jupp, 2009; Paine et al., 2020). A regression method for analyzing such data was first introduced in Chang (1986), and subsequent developments include (Downs, 2003; Rosenthal et al., 2014; Scaaly and Wood, 2019; Paine et al., 2020), and few other approaches are proposed relying on the properties of homogeneous Riemannian manifold (Hinkle et al., 2014; Cornea et al., 2017). Pewsey and García-Portugués (2021) provided a thorough review in this context. Nevertheless, none of these approaches are suitable for studying spatially varying directional outcomes.

In this paper, we develop a novel regression approach to infer the effects of several external factors on spatially varying directional data as an outcome. Notationally, let a p -variate directional data measured at the replication i and location v , denoted as $\mathbf{E}_{iv} \in \mathcal{S}^{p-1}$, be the outcome of interest, and let a covariate vector $\mathbf{X}_i = [1, X_{i1}, \dots, X_{ic}, \dots, X_{iC}]$ represent the array of predictors. Here \mathcal{S}^{p-1} stands for the p -dimensional sphere. Our objective is to regress \mathbf{E}_{iv} on \mathbf{X}_i for statistical inference purposes. In summary, we propose a generalized regression model for unit vector-valued responses, incorporating a novel link function based on the transformation between Cartesian and spherical coordinates. This link function enables us to project the directional data onto Euclidean space, thus allowing us to efficiently model the covariate effects.

As discussed in Paine et al. (2020), the regression models for angular data or \mathcal{S}^1 are not easily extended for \mathcal{S}^2 or higher dimensional spheres. The fact that the intercept takes care of the rotational invariance as in Fisher and Lee (1992) is very specific to the angular data only. In our model, such modification would not make the estimate rotation invariant as the response is in \mathcal{S}^2 . Following model Structure 2 of Paine et al. (2020) and Section 4.3.1 of Scaaly and Wood (2019), we add an unknown rotation matrix \mathbf{Q} as a parameter that allows the inference to not depend on the coordinate system. Unlike Scaaly and Wood (2019), we put a prior and sample this orthogonal matrix within our MCMC

since in a spatial setting, their approach for the pre-specification of this matrix may not be appropriate. Thus, the posterior samples of the regression coefficients become dependent on the posterior samples of the orthogonal matrix. Thus, it remains not straightforward to use the regression coefficients directly for *scientific* inference. Thus, we consider a tangent-normal decomposition-based inference framework instead of using the regression coefficients directly. Specifically, we summarize the change in directional-valued mean upon a one-unit change in predictors in terms of the magnitude of the tangent-normal component and use those summarizations to quantify the importance of different predictors. Further details are provided in Section 3. Moreover, the inclusion of this orthogonal matrix improves flexibility along the lines of Kent et al. (2006); Scaely and Wood (2019); Paine et al. (2020) and also the model performance, as shown in our simulation results in Section 4.

Another important component to be addressed is the aspect of complex spatial dependence. In many modern applications, the directional data are spatially correlated, and the spatial dependence presents a different and unique pattern, i.e., the spatial dependence of this type of directional data is usually along *streamlines* (Yeatman et al., 2012). The *streamlines* have different meanings in different applications. In animal migration, *streamlines* are the animal migration pathways (Mahan, 1991). In DTI, the *streamlines* are the fiber *streamlines*, i.e., the blue curves in the middle panel of Figure 1. In Goodlett et al. (2009); Zhu et al. (2011), the authors proposed methods that induce spatial dependence by considering arc length distances along a fiber while analyzing the fiber orientation data. Such dependence can be observed in our motivating DTI data (see Section A.1 in the supplementary materials) too. Motivated by this, we impose the spatial dependence along the *streamlines*, relying on an autoregressive model. For our Alzheimer’s Disease Neuroimaging Initiative (ADNI) data analysis, the fiber *streamlines*, based on the tractography atlases from Yeh et al. (2018) are used. The tractography atlases provided by Yeh et al. (2018) offer inter-voxel connectivities along a given fiber tract fornix (see Figure 2). These are es-

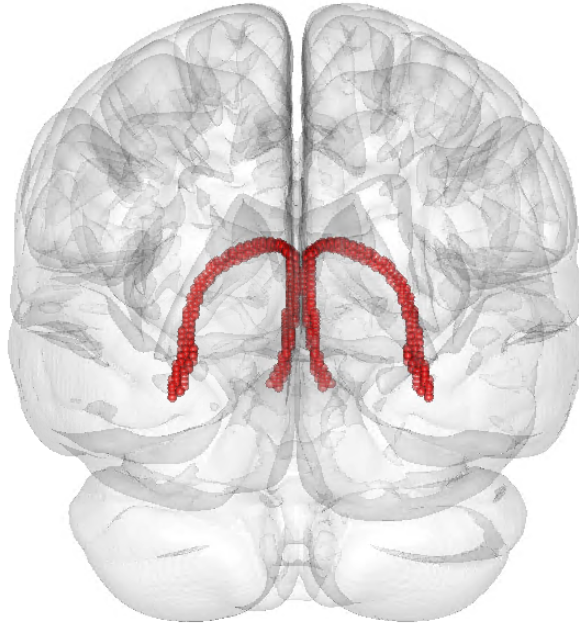


Figure 2: Tractography atlas of fornix .

estimated using high-quality diffusion-weighted images from healthy subjects. Fornix’s tract profile has been studied in many other studies (Valdés Cabrera et al., 2020; Cahn et al., 2021).

In the rest of the paper, we first illustrate the model construction in Section 2. The proposed Bayesian angular inference is given in Section 3. To evaluate the performance of our model, we provide numerical studies in Section 4. Finally, we conclude and discuss in Section 5. Supplementary figures and computational materials are in supplementary materials.

2 Model Construction

In this section, we provide the details of the model construction. Section 2.1 describes the distribution that serves as the noise model for directional data. Subsequently, Section 2.2 introduces the link function, which allows us to relate a linear combination of the predictors to the response variables. Finally, we describe the model for spatial dependence in Section

2.3.

2.1 vMF Distribution

A random p -dimensional directional data point, \mathbf{E}_{iv} , lies on \mathcal{S}^{p-1} , as described in Section 1. The von Mises-Fisher (vMF) distribution (Mardia and Jupp, 2009) is a commonly used probability distribution for handling directional data, and spherical regression models are built based on the vMF distribution. However, building spherical regression models is not straightforward since the inference might depend on an arbitrary coordinate system in which the responses are defined. Following the approaches in Scealy and Wood (2019); Paine et al. (2020), We assume that $\mathbf{Q}^T \mathbf{E}_{iv}$ follows a von Mises-Fisher (vMF) distribution (Mardia and Jupp, 2009), denoted as $\mathbf{Q}^T \mathbf{E}_{iv} \sim \text{vMF}(\boldsymbol{\mu}_{iv}, \kappa)$ with the probability density function expressed as

$$f[\mathbf{Q}^T \mathbf{E}_{iv} | \boldsymbol{\mu}_{iv}, \kappa] = C_p(\kappa) \exp\left(\kappa \boldsymbol{\mu}_{iv}^T \mathbf{Q}^T \mathbf{E}_{iv}\right) = C_p(\kappa) \exp\left(\kappa \mathcal{M}_{iv}^T \mathbf{E}_{iv}\right), \quad (1)$$

In the expression, $C_p(\kappa)$ is the normalizing constant such as $C_p(\kappa) = \frac{\kappa^{p/2-1}}{(2\pi)^{p/2} I_{p/2-1}(\kappa)}$, where I_a stands for the modified Bessel function of the first kind at order a . In this paper, we primarily focus on the case with $p = 3$, due to the nature of the DTI data, and in that case, $C_3(\kappa) = \frac{\kappa}{2\pi(e^\kappa - e^{-\kappa})}$ and the density simplifies to $\frac{\kappa \exp(\kappa(\boldsymbol{\mu}^T \mathbf{x} - 1))}{2\pi(1 - \exp(-2\kappa))}$ for a point $\mathbf{x} \in \mathcal{S}^2$. There are some pictorial illustrations available in Straub (2017). The term $\boldsymbol{\mu}_{iv}$ is a directional vector, i.e., $\|\boldsymbol{\mu}_{iv}\| = 1$, where $\|\cdot\|$ represents the ℓ_2 norm. $\kappa \geq 0$ is a concentration parameter. The term \mathbf{Q} is set as an unknown parameter in our model and modeled as a special orthogonal matrix.

The density is maximized at $\mathbf{E}_{iv} = \mathbf{Q} \boldsymbol{\mu}_{iv}$, the mode direction parameter. Thus, we further introduce the notation

$$\mathcal{M}_{iv} = \mathbf{Q} \boldsymbol{\mu}_{iv}, \quad (2)$$

and it is the mode direction for the *original* response \mathbf{E}_{iv} , and is named as *direct* mode

direction to differentiate it from $\boldsymbol{\mu}_{iv}$ which is called *rotated* mode direction. In the next subsection, we propose a link function to relate predictors with $\boldsymbol{\mu}_{iv}$. Since the link function is known and pre-specified, the orthogonal matrix \mathbf{Q} here provides additional flexibility by identifying an optimal coordinate system with respect to the link.

2.2 Linking to Predictors

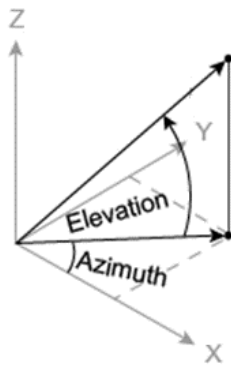
In accordance with the generalized linear regression (GLM) framework, we propose a relationship between a linear combination of the predictors and the response variables through a link function. It is also reasonable to allow the linear combination of the predictors to be unbounded, mirroring other GLM frameworks. Therefore, our proposed link function is a composition of two functions, each handling a different level of transformations. The following section provides detailed insight into the construction of the link function.

In this section, we focus on our link function for 3-dimensional spherical coordinates, i.e., when \mathbf{E}_{iv} lies on \mathcal{S}^{p-1} and $p = 3$. Let (x, y, z) represent the Cartesian coordinates of a point on the sphere such that $x^2 + y^2 + z^2 = 1$. This point can be represented in spherical coordinates using two parameters, as depicted in Figure 3a. The azimuth angle $\theta \in (-\pi, \pi]$ represents the counterclockwise angle in the x-y plane from the positive x-axis, and the elevation angle $\phi \in (-\frac{\pi}{2}, \frac{\pi}{2}]$ is the angle from the x-y plane. The one-to-one transformation from Cartesian to spherical coordinates is as follows:

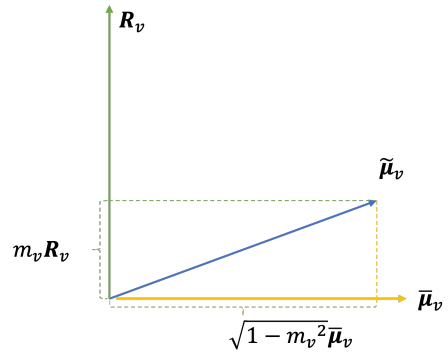
$$u : (x, y, z) \rightarrow \left(\text{atan2}(y, x), \text{atan2}(z, \sqrt{1 - z^2}) \right) = (\theta, \phi),$$

where $\text{atan2}(y, x)$ is defined by the limit expression $\lim_{z \rightarrow x^+} \left(\frac{y}{z} \right) + \frac{\pi}{2} \text{sgn}(y) \text{sgn}(x) (\text{sgn}(x) - 1)$. While the spherical coordinates (θ, ϕ) are located in Euclidean space, they are bounded. Hence, we first scale the spherical coordinates (θ, ϕ) to fall within the interval $(0, 1]$, then apply the logit function. The transformation is:

$$g : (\theta, \phi) \rightarrow \left(\text{logit}\left(\frac{\theta + \pi}{2\pi}\right), \text{logit}\left(\frac{\phi + \pi/2}{\pi}\right) \right) = (\tilde{\theta}, \tilde{\phi}) \in \mathbb{R} \times \mathbb{R}.$$



(a) The graphical illustration describes the transformation between Cartesian and spherical coordinates. The azimuth angle and elevation angle are labeled in the Cartesian coordinate system.



(b) The graphical illustration of tangent-normal decomposition of covariate effects. The yellow arrow is the *typical* mode direction; the blue arrow is the *specific* mode direction; the green arrow is the *deviation* direction; The scalar $m_v \in (0, 1)$ controls the magnitude of this effect.

Figure 3: The graphical illustrations of directional statistics.

Here, $\text{logit}(x) = \log\left(\frac{x}{1-x}\right)$. Although the logit transformation ill-behaves on the boundary (i.e., at $x = 1$), the regression model built on this transformation is still adequately flexible, as the set of such degenerate cases has measure zero. This transformation serves to map the bounded spherical coordinates to a new set of parameters $(\tilde{\theta}, \tilde{\phi})$, which are unbounded. For clarity, the overall mapping from (x, y, z) to $(\tilde{\theta}, \tilde{\phi})$ is denoted by $\ell(\cdot)$, which is a composite of $g(\cdot)$ and $u(\cdot)$, i.e., $\ell(\cdot) := u(\cdot) \circ g(\cdot)$. Thus, $\ell(x, y, z) = [\tilde{\theta}, \tilde{\phi}]$ represents this innovative function that projects the directional data from \mathcal{S}^2 to $\mathbb{R} \times \mathbb{R}$.

A point on a p dimensional hypersphere, \mathcal{S}^{p-1} , can be expressed using $p - 1$ angles. The first $p - 2$ angles (denoted as $\boldsymbol{\phi}^{(p-2)} = [\phi_1^{(p-2)}, \dots, \phi_{p-2}^{(p-2)}]$) are within the interval $(-\pi/2, \pi/2]$, while the last angle θ is within $(-\pi, \pi]$. The mapping function, when extended to the general dimension, is formulated as:

$$\begin{aligned} g : (\theta, \boldsymbol{\phi}^{(p-2)}) &\rightarrow \left(\text{logit}\left(\frac{\theta + \pi}{2\pi}\right), \left[\text{logit}\left(\frac{\phi_1^{(p-2)} + \pi/2}{\pi}\right), \dots, \text{logit}\left(\frac{\phi_{p-1}^{(p-2)} + \pi/2}{\pi}\right) \right] \right) \\ &= (\tilde{\theta}, [\tilde{\phi}_1^{(p-2)}, \dots, \tilde{\phi}_{p-2}^{(p-2)}]) \in \mathbb{R} \times \mathbb{R}^{p-2}. \end{aligned}$$

In our proposed generalized regression model, the link function $\ell(\cdot)$ plays a key role. The term $\ell(\boldsymbol{\mu}_{iv}) = (\tilde{\theta}, [\tilde{\phi}_1^{(p-2)}, \dots, \tilde{\phi}_{p-2}^{(p-2)}])$ is considered as the prediction terms and is formulated as a function of the covariate vector \mathbf{X}_i . Specifically, we have:

$$\mathbb{E}(\tilde{\theta}, [\tilde{\phi}_1^{(p-2)}, \dots, \tilde{\phi}_{p-2}^{(p-2)}]) = (\mathbf{X}_i \boldsymbol{\alpha}_v, [\mathbf{X}_i \boldsymbol{\beta}_{v,1}^{(p-2)}, \dots, \mathbf{X}_i \boldsymbol{\beta}_{v,p-2}^{(p-2)}]).$$

Lemma 1 illustrates that the link function $\ell(\cdot)$ is a bijective function. This provides us with a direct mapping between the coordinates $(\tilde{\theta}, [\tilde{\phi}_1^{(p-2)}, \dots, \tilde{\phi}_{p-2}^{(p-2)}])$ and the mode direction $\boldsymbol{\mu}_{iv}$. This mapping is crucial in facilitating the interpretation of the regression coefficients.

Lemma 1. *The function $\ell(\cdot) : \mathcal{S}^{p-1} \rightarrow \mathbb{R}^{p-2} \times \mathbb{R}$ is bijective.*

Proof. We know $\ell(\cdot) := u(\cdot) \circ g(\cdot)$ where \circ is function composition. Since $u(\cdot)$ and $g(\cdot)$ are both bijective, $\ell(\cdot)$ is bijective. \square

For the remainder of this article, in view of our DTI application and to simplify the exposition, we set $p = 3$, i.e.,

$$\mathbb{E}[\tilde{\theta}_{iv}, \tilde{\phi}_{iv}]^T = [\mathbf{X}_i \boldsymbol{\alpha}_v, \mathbf{X}_i \boldsymbol{\beta}_v]^T,$$

and drop the superscript $(p - 2)$. Despite this simplification, it should be noted that it is straightforward to generalize all the steps we take here to accommodate any general p .

2.3 Spatial Dependence

Spatial dependence is an essential component in many applications. In this section, we further illustrate the model specification which accounts for spatial dependence. By preserving $\mathbb{E}[\tilde{\theta}_{iv}, \tilde{\phi}_{iv}]^T = [\mathbf{X}_i \boldsymbol{\alpha}_v, \mathbf{X}_i \boldsymbol{\beta}_v]^T$, we let $[\tilde{\theta}_{iv}, \tilde{\phi}_{iv}]^T = [\mathbf{X}_i \boldsymbol{\alpha}_v + \boldsymbol{\epsilon}_{iv}, \mathbf{X}_i \boldsymbol{\beta}_v + \boldsymbol{\xi}_{iv}]^T$, where $\boldsymbol{\epsilon}_i = (\epsilon_{1i}, \dots, \epsilon_{iv}, \dots, \epsilon_{iV})$ and $\boldsymbol{\xi}_i = (\xi_{1i}, \dots, \xi_{iv}, \dots, \xi_{iV})$ are distributed as the mean-zero Gaussian distribution with covariance matrices $\boldsymbol{\Sigma}^{(\epsilon)}$ and $\boldsymbol{\Sigma}^{(\xi)}$, respectively.

The focus of our applications is principal directional data where the spatial dependence is along a given fiber streamline. Suppose we have K fiber streamlines, \mathbb{Z}_k is a set of consecutive indices within the k -th fiber streamline. We let the directional statistics are auto-correlated along a given streamline. For completeness, we first state the definition and notations related to the Gaussian autoregressive modeling in Definition 1.

Definition 1 (AR(P) Process). *Given $A_t = A_{t-1}\Phi_1 + \dots + A_{t-P}\Phi_P + \epsilon_t$ and $\epsilon_t \sim \mathcal{N}(0, \sigma^2)$, for $t \in \mathbb{Z}$. For $t \in \mathbb{Z}$, we define that $\{A_t : t \in \mathbb{Z}\}$ follows a Gaussian AR- P process with correlation parameters (Φ_1, \dots, Φ_P) and variance σ^2 , denoted as $AR_P([\Phi_1, \dots, \Phi_P], \sigma^2)$.*

We thus have $\boldsymbol{\epsilon}_i = (\epsilon_{1i}, \dots, \epsilon_{iv}, \dots, \epsilon_{iV})$ and $\boldsymbol{\xi}_i = (\xi_{1i}, \dots, \xi_{iv}, \dots, \xi_{iV})$ follow a multivariate normal distribution with an autoregressive covariance matrix, denoted as

$$\begin{aligned} \boldsymbol{\epsilon}_{ik} &= \{\epsilon_{iv} : v \in \mathbb{Z}_k\} \sim AR_P([\Phi_{\epsilon 1}, \dots, \Phi_{\epsilon P}], \tau_{\epsilon}^2) \\ \boldsymbol{\xi}_{ik} &= \{\xi_{iv} : v \in \mathbb{Z}_k\} \sim AR_P([\Phi_{\xi 1}, \dots, \Phi_{\xi P}], \tau_{\xi}^2), \end{aligned} \tag{3}$$

where $(\Phi_{\epsilon,1}, \dots, \Phi_{\epsilon,P}, \tau_{\epsilon}^2)$ and $(\Phi_{\xi,1}, \dots, \Phi_{\xi,P}, \tau_{\xi}^2)$ are the corresponding parameters. Note that our characterization of the AR(P) process is based on the partial correlations but not the autoregressive coefficients directly.

2.4 Prior Settings

We now put priors on the model parameters to proceed with our Bayesian inference. The matrix \mathbf{Q} is first reparametrized using the Cayley transformation as $\mathbf{Q} = (\mathbf{I} - \mathbf{A})(\mathbf{I} + \mathbf{A})^{-1}$, where \mathbf{A} is a skew-symmetric matrix. This parametrization is useful for efficient posterior computation. Setting $\mathbf{A} = \begin{bmatrix} 0 & a_1 & a_2 \\ -a_1 & 0 & a_3 \\ -a_2 & -a_3 & 0 \end{bmatrix}$, the priors for the three parameters a_1, a_2, a_3 are set as mean-zero normal with variance 100. For the regression coefficients, we also assign AR- P process priors, denoted as

$$\begin{aligned} \boldsymbol{\alpha}_k(c) &= \{\alpha_v(c) : v \in \mathbb{Z}_k\} \sim \text{AR}_P([\Phi_{\alpha,1}, \dots, \Phi_{\alpha,P}], \sigma_{\alpha}^2) \\ \boldsymbol{\beta}_k(c) &= \{\beta_v(c) : v \in \mathbb{Z}_k\} \sim \text{AR}_P([\Phi_{\beta,1}, \dots, \Phi_{\beta,P}], \sigma_{\beta}^2), \end{aligned} \tag{4}$$

where $\boldsymbol{\alpha}_v = (\alpha_v(0), \dots, \alpha_v(c), \dots, \alpha_v(C))$ and $\boldsymbol{\beta}_v = (\beta_v(0), \dots, \beta_v(c), \dots, \beta_v(C))$. The terms $\alpha_v(0)$ and $\beta_v(0)$ are the coefficients for the intercepts. The terms $\alpha_v(c)$ and $\beta_v(c)$ are the coefficients for the covariate c . The variances are assigned with weakly informative inverse-gamma priors with shape and rate parameters set to 0.1, denoted as $\tau_{\epsilon}^{-2}, \tau_{\xi}^{-2}, \sigma_{\alpha}^{-2}, \sigma_{\beta}^{-2} \sim \mathcal{GA}(0.1, 0.1)$. We put a diffuse prior for the concentration parameter, κ , denoted as $\kappa \propto 1$. The concentration parameter κ can be viewed as a nugget effect. An autoregressive process with the partial autocorrelation parameters restricted to $(-1, 1)$ can ensure stationarity (Barnett et al., 1996). Therefore, we assign uniform $(-1, 1)$ prior on the partial autocorrelation parameters. Specifically, $\rho_{\alpha,p}, \rho_{\beta,p}, \rho_{\epsilon,p}, \rho_{\xi,p} \sim \mathcal{U}(-1, 1)$ for $p \in \{1, 2, \dots, P\}$, where $\rho_{\alpha,p}, \rho_{\beta,p}, \rho_{\epsilon,p}, \rho_{\xi,p}$ are the corresponding partial autocorrelation parameters associated with the autoregressive process priors for $\boldsymbol{\alpha}_v(c)$'s, $\boldsymbol{\beta}_v(c)$'s, and the

autoregressive random effects ϵ_{ik} 's, and ξ_{ik} 's, respectively. Applying the Durbin-Levinson recursion on the partial autocorrelations $(\rho_{\alpha,p}, \rho_{\beta,p}, \rho_{\epsilon,p}, \rho_{\xi,p})$, we get back the autoregressive coefficients $(\Phi_{\alpha,p}, \Phi_{\beta,p}, \Phi_{\epsilon,p}, \Phi_{\xi,p})$ using the R function `inla.ar.pacf2phi()` from the R package `inla` (Lindgren and Rue, 2015). The reverse transformation is applied using `inla.ar.phi2pacf()` from the same package. We utilize a Markov chain Monte Carlo (MCMC) algorithm, which includes Metropolis-Hastings-within-Gibbs steps, to generate the posterior samples needed for our Bayesian inference. The codes and usages of our codes are stated in Section B.1. of the supplementary materials.

3 Bayesian Angular Inference

In this section, we present our novel Bayesian angular inference framework for directional data analysis. The interpretation of the regression coefficients in our model is not as straightforward as it is in linear regression. The proposed inferential framework aims to address this complexity in inference. The main difficulty arises when trying to illustrate the effects of covariates. In Section 3.2, we illustrate our approach for characterizing the effects of the covariates. This relies on a suitable metric for performing inferences based on directional statistics. For clarity, Section 3.1 first introduces the angular expectation formula which is going to be the metric in the later part. These approaches aim to improve our understanding and analysis of complex directional data.

3.1 Angular Expectation

For a random unit vector \mathcal{M} , the angular expectation is defined as

$$\mathbb{A}\mathcal{M} = \arg \min_{\mathbf{m} \in \mathcal{S}^{p-1}} \int \delta(\mathbf{m}, \mathcal{M}) \pi(\mathcal{M}) d\mathcal{M},$$

where \mathbb{A} is introduced as an operator returning the angular expectation, p is the dimension of \mathcal{M} , and $\pi(\mathcal{M})$ stands for the distribution of \mathcal{M} . The angular expectation \mathbb{A} is the

main tool for our proposed Bayesian angular inference scheme. For a new subject with the covariate vector \mathbf{X}_{new} , the posterior predictive distribution of the *direct* mode direction $\boldsymbol{\mu}_{\text{new},v}$ for the v -th index (Equation 2), is $\left[\mathcal{M}_{\text{new},v}|\mathbf{X}_{\text{new}};\text{data}\right]$. For clarity, we use subscript “new” to replace the original subscript “ i ” in the model for referring to a new subject. For summarizing above posterior of $\mathcal{M}_{\text{new},v}$, we compute the posterior angular expectation using the MCMC samples $\{\mathcal{M}_{\text{new},v}^{(t)} : t = 1 : T\}$ as

$$\mathbb{A}\left[\mathcal{M}_{\text{new},v}|\mathbf{X}_{\text{new}};\text{data}\right] \approx \arg \min_{\mathbf{m} \in \mathcal{S}^{p-1}} \frac{1}{T} \sum_{t=1}^T \delta(\mathbf{m}, \mathcal{M}_{\text{new},v}^{(t)}) = \frac{\sum_{t=1}^T \mathcal{M}_{\text{new},v}^{(t)}/T}{\|\sum_{t=1}^T \mathcal{M}_{\text{new},v}^{(t)}/T\|}.$$

Relating to the real applications, the above term profiles the expected fiber direction after the model-based adjustment for the covariate vector \mathbf{X}_{new} .

3.2 Tangent-Normal Decomposition to Investigate Covariate Effects

A transparent inference framework illustrating the covariate effects is essential for any scientific study. In our proposed model, the coefficients $\boldsymbol{\alpha}_v$ and $\boldsymbol{\beta}_v$ do not offer a straightforward illustration of the covariate effects on the mode directions. This is also a limitation of many regression models for complicated responses. To overcome this, we incorporate the tangent-normal decomposition (Mardia and Jupp, 2009, Page 169) to summarize the covariate effects on directional data as follows. The tangent-normal decomposition is an integrated approach, but can be decomposed into the following three steps for a concise illustration.

Our proposed procedure starts by defining the following two covariate vectors: a) $\mathbf{X}_{\text{T}} = [1, X_{\text{T}1}, \dots, X_{\text{T}c}, \dots, X_{\text{T}C}]$: Covariate vector for the *typical* condition; b) $\mathbf{X}_{\text{S}} = [1, X_{\text{S}1}, \dots, X_{\text{S}c}, \dots, X_{\text{S}C}]$: Covariate vector for the *specific* condition. Thus, we replace the original subscript “ i ” with “T” and “S” in our notation, to represent a subject in the *typical* and *specific* condition, respectively.

Next, we obtain the corresponding predictive posterior distributions of the mode directions with the given *typical* or *specific* covariate vector. They are referred as to the *typical* and *specific* mode direction, respectively, expressed as follows: a) *Typical* Mode Direction: $\overline{\mathcal{M}}_v = [\mathcal{M}_{T_v} | \mathbf{X}_T; \text{data}]$; b) *Specific* Mode Direction: $\widetilde{\mathcal{M}}_v = [\mathcal{M}_{S_v} | \mathbf{X}_H; \text{data}]$. They can also be approximately learned from the MCMC output through the \mathbb{A} operator defined above.

To quantify the covariate effect, we employ the tangent-normal decomposition on the *specific* mode direction $\widetilde{\mathcal{M}}_v$ as in Figure 3b where the *typical* mode direction $\overline{\mathcal{M}}_v$ is the tangent direction and the term \mathbf{R}_v is the normal direction. Applying this to the principal diffusion directions, the term \mathbf{R}_v can be interpreted as the *deviation* direction that is caused by the difference from the *specific* condition to the *typical* condition. The scalar $m_v \in (0, 1)$, which controls the magnitude of this effect, can be used to quantify the importance of this covariate: the larger value of m_v indicates the stronger deviation between the *specific* condition to the *typical* condition. Computationally, the tangent-normal decomposition can be applied to each MCMC sample t . This provides us with the posterior samples of \mathbf{R}_v and m_v , denoted as $\{\mathbf{R}_v^{(t)} : t = 1 : T\}$ and $\{m_v^{(t)} : t = 1 : T\}$. We use those samples to obtain posterior estimates of $\mathbb{A}[\mathbf{R}_v | \text{data}]$ to spatially profile the *deviation* directions caused by the difference between *typical* condition and *specific* condition. Similarly, the posterior mean estimate of m_v can also be computed and used to quantify the magnitude. We use the following notation to express the tangent-normal decomposition:

$$\mathcal{D}_{TN}(\overline{\mathcal{M}}_v || \widetilde{\mathcal{M}}_v) = \{\mathbf{R}_v, m_v\} \quad (5)$$

Our above illustration provides the general description of tangent-normal decomposition. As long as it is feasible to specify the *typical* and *specific* conditions, they may use $\{\mathbf{R}_v, m_v\}$ to infer the covariate effects caused by the difference between the *typical* and *specific* conditions. The below are two important remarks which are important for the

general use of our approach.

Remark 1. *Two covariate vectors can be any two conditions where we want to compare the specific condition “to” the typical condition which is considered as reference. Usually, \mathbf{X}_T is set to the common characterization.*

Remark 2. $\mathcal{D}_{TN}(\overline{\mathcal{M}}_v || \widetilde{\mathcal{M}}_v)$ is not symmetric in the two inputs, i.e., $\mathcal{D}_{TN}(\overline{\mathcal{M}}_v || \widetilde{\mathcal{M}}_v) \neq \mathcal{D}_{TN}(\widetilde{\mathcal{M}}_v || \overline{\mathcal{M}}_v)$. Thus, the specific condition and the typical condition cannot be exchanged.

While we illustrate the use of our approach as a generic use, interpreting one covariate effect at a time is usually a common manner. Therefore, we further provide two examples below to illustrate how to interpret one covariate effect at a time. In summary, the key strategy is to have *typical* and *specific* conditions differ only in the covariate c' of our primary interest.

Example 1 (Continuous Covariate). *Let c' represent a continuous covariate. The terms $X_{T_{c'}}$ and $X_{S_{c'}}$ correspond to the values in the typical and the specific cases, respectively. When investigating the impact of a single unit increase in the covariate c' , with $X_{T_{c'}} = a$, we assign $X_{S_{c'}} = a + 1$. Concurrently, we ensure $X_{S_c} = X_{T_c}$ for all other c variables.*

Example 2 (Categorical Covariate). *Let c' represent a categorical covariate with M levels, where $m \in 1, \dots, M$. The terms $\{X_{T_{c'},m}\} \in \{0, 1\}$ and $\{X_{S_{c'},m}\} \in \{0, 1\}$ denote the corresponding specification for level m . Specifically, $X_{T_{c'},j} = 1$ and $X_{S_{c'},j'} = 1$ if the typical case is categorized under the j -th level and the specific condition falls under the j' -th level. This is with the condition that $X_{T_{c'},m} = 0$ for all $m \neq j$, and $X_{S_{c'},m} = 0$ for all $k \neq j'$. In assessing the impact of the j' -th level starting from a typical case in the j -th level, we set $X_{S_{c'},j'} = 1$ and $X_{T_{c'},j} = 1$, while ensuring $X_{S_c} = X_{T_c}$ for all the other $c \in \{0 : C\}$ variables.*

4 Numerical Studies

In this section, we aim to demonstrate the efficacy of our model compared to traditional methods. Initially, we evaluate our model fitness on synthetic data in Section . We generate the synthetic data to best mimic the real ADNI data.

The ADNI initiative was inaugurated in 2003 as a public-private partnership with the primary goal of assessing whether the amalgamation of serial magnetic resonance imaging, positron emission tomography, other biological markers, and clinical as well as neuropsychological assessments could aid in predicting the progression of Alzheimer’s disease. This paper specifically focuses on ADNI-2, a project that commenced in September 2011 and spanned five years (Aisen et al., 2010). The Centers for Disease Control and Prevention (<https://www.cdc.gov/aging/aginginfo/alzheimers.htm>) suggests that Alzheimer’s disease symptoms typically occur after the age of 60. Therefore, we have tailored our study cohort to focus on subjects over 60 years old. The subjects are further classified into four disease states: healthy controls (CN), early mild cognitive impairment (EMCI), late mild cognitive impairment (LMCI), and Alzheimer’s Disease (AD). We use $g \in \{\text{CN}, \text{EMIC}, \text{LMCI}, \text{AD}\}$ to denote the group index.

Additionally, we collect subject-level information including age ($X_{i,age}$), gender ($X_{i,gender}$), mini-mental state examination (MMSE) score ($X_{i,MMSE}$), and the Apolipoprotein E (APOE) profile ($X_{i,APOE}$). The MMSE is a performance-based neuropsychological test score ranging from 0 to 30. Subjects with cognitive impairments are typically associated with a lower MMSE score. The APOE is a genetic marker with three major variants (ϵ -2, ϵ -3, and ϵ -4). The ϵ -4 variant is considered the most significant known genetic risk factor for Alzheimer’s disease across various ethnic groups (Sadigh-Eteghad et al., 2012). Consequently, our analysis includes APOE-4 as a binary indicator, which denotes the presence of the ϵ -4 variant in subjects. We also incorporate age and gender into our analysis, given that previous

studies have established their correlation with AD (Podcasy and Epperson, 2022). In Section 4.1, we provide the model comparison based on both synthetic data and real ADNI data. In Section 4.2, we provide the tangent-normal decomposition within Bayesian angular inference to infer the covariate effects. In both sections, we make the design matrix as

$$\mathbf{X}_i = [1, X_{i,age}, X_{i,gender}, X_{i,MMSE}, X_{i,APOE}] \quad (6)$$

We further specify the regression terms as

$$\mathbb{E}\ell(\boldsymbol{\mu}_{iv}) = \mathbb{E}[\tilde{\boldsymbol{\theta}}_{iv}, \tilde{\boldsymbol{\phi}}_{iv}]^T = [\mathbf{X}_i \boldsymbol{\alpha}_{gv}, \mathbf{X}_i \boldsymbol{\beta}_{gv}]^T \quad \text{for subject } i \text{ in clinical group } g. \quad (7)$$

In this way, the covariate effects are clinical group-specific.

4.1 Model Comparison

In this section, we carry out numerical analyses on both the ADNI data and synthetic principal diffusion direction data. The purpose of these studies is to demonstrate the superior performance of our proposed vMF regression relative to other methods. Here, we consider three competing methods based on multivariate Gaussian distribution: 1) *Gaussian Regression 1*: a multivariate regression model for the principal diffusion directions \mathbf{E}_{iv} , 2) *Gaussian Regression 2*: a multivariate regression model for transformed means $\ell(\mathbf{E}_{iv})$, 3) *Non-spatial vMF regression*: $\mathbf{Q}^T \mathbf{E}_{iv} \sim \text{vMF}(\mathcal{M}_{iv}, \kappa)$ and $\ell(\boldsymbol{\mu}_{iv}) = [\tilde{\boldsymbol{\theta}}_{iv}, \tilde{\boldsymbol{\phi}}_{iv}]^T = [\mathbf{X}_i \boldsymbol{\alpha}_{gv}, \mathbf{X}_i \boldsymbol{\beta}_{gv}]^T$. Specific details are described as follows. The *Gaussian Regression 1* simply treats the principal diffusion directions \mathbf{E}_{iv} as normally distributed random variables, such that $\mathbf{E}_{iv} \sim \mathcal{N}(\mathcal{M}_{iv}, \boldsymbol{\Sigma}_1)$, where $\mathcal{M}_{iv}^{(p)} = \mathbf{X}_i \mathbf{u}_v^{(p)}$, $\mathcal{M}_{iv}^{(p)}$ is the p -th element of \mathcal{M}_{iv} for $p \in \{1, 2, 3\}$, i.e., $\mathcal{M}_{iv} = (\mathcal{M}_{iv}^{(1)}, \mathcal{M}_{iv}^{(2)}, \mathcal{M}_{iv}^{(3)})$. Alternatively, in case of *Gaussian Regression 2*., the terms $\ell(\mathbf{E}_{iv}) = [A_{iv}, B_{iv}]^T$ are assumed to follow a normal distribution, denoted as $\ell(\mathbf{E}_{iv}) = [A_{iv}, B_{iv}]^T \sim \mathcal{N}([\tilde{\boldsymbol{\theta}}_{iv}, \tilde{\boldsymbol{\phi}}_{iv}]^T, \boldsymbol{\Sigma}_2)$, where $\tilde{\boldsymbol{\theta}}_{iv} = \mathbf{X}_i \mathbf{a}_v$ and $\tilde{\boldsymbol{\phi}}_{iv} = \mathbf{X}_i \mathbf{b}_v$. In case of

Non-spatial vMF Regression:, we simply remove the spatially dependent randomness from the proposed model.

We take the Bayesian route for inference for all these methods and put weakly informative priors on the unknown parameters. Specifically, we give normal priors with mean $\mathbf{0}$ and covariance matrix $1000 \times \mathbf{I}$ on the coefficients, denoted as $\mathbf{u}_v^{(1)}, \mathbf{u}_v^{(2)}, \mathbf{u}_v^{(3)}, \mathbf{a}_v, \mathbf{b}_v \sim \mathcal{N}(\mathbf{0}, 1000 \times \mathbf{I})$. We further put inverse Wishart prior with degrees of freedom 5 and scale matrix \mathbf{I} on the covariance matrices, denoted as $\Sigma_1^{-1}, \Sigma_2^{-1} \sim \mathcal{W}(5, \mathbf{I})$. Our inference is based on the posterior samples, generated by applying the MCMC algorithm, where we collect 3,000 post-burn samples after discarding the first 2,000. The MCMC convergence is monitored by Heidelberger and Welch’s convergence diagnostic (Heidelberger and Welch, 1981).

We generate synthetic principal diffusion direction data using our proposed vMF regression model. We design a synthetic fiber tract that includes $K = 12$ fibers and a total of 1,256 voxels. We also have covariate vectors for 20 subjects for training and 20 subjects for validation. For each data replication, we fit our model to the training data to obtain the parameter estimates and these parameter estimates are used to predict the response in the validation data. The discrepancies between the predict the responses and true responses are used to measure model accuracy.

The tractography atlas, values of covariate vectors and voxel-wise coefficients utilized are stored in the R file `synthetic.Rdata`, as detailed in Section B.2 of the supplementary materials. For other parameters, we set $P = 5$ and generate partial correlation coefficients from $\mathcal{U}(-1, 1)$. The variances are specified as $\tau_\epsilon^2 = \tau_\xi^2 = \sigma_\alpha^2 = \sigma_\beta^2 = 1$, and orthogonal matrix is specified as $\mathbf{Q} = \mathbf{I}$. We further give $\kappa \in \{20, 30, 40\}$, respectively. A total of 50 replicated data sets for each setting.

Prediction errors are quantified in terms of a) the separation angle b) the root mean squared error. The separation angle is defined as $\sum_{i,v} \delta(\widehat{\mathcal{M}}_{iv}, \mathbf{E}_{iv})/N_{iv}$ for vMF regression

and $\sum_{i,v} \delta(\widehat{\mathcal{M}}_{iv}, \mathbf{E}_{iv})/N_{iv}$ for Gaussian regression methods. The root mean squared error is defined as $\sum_{i,v} \|\widehat{\mathcal{M}}_{iv} - \hat{\mathbf{Q}}^T \mathbf{E}_{iv}\|/N_{iv}$ for vMF regression and $\sum_{i,v} \|\widehat{\mathcal{M}}_{iv}/\|\widehat{\mathcal{M}}_{iv}\| - \mathbf{E}_{iv}\|/N_{iv}$ for Gaussian case. We give the prediction errors spanning simulation replications in Figure 4. Our proposed method substantially outperforms Gaussian alternatives and the non-spatial vMF regression model based on these prediction errors. The spatial vMF regression with $P = 5$ demonstrates comparatively better performance among $P \in \{2, \dots, 7\}$. This aligns with the fact that true data is generated by setting $P = 5$. It suggests that the optimal lag can be chosen based on the predictive performances for our real data analysis.

4.2 Bayesian Angular Inference for ADNI Data

In this section, we utilize our Bayesian angular inference method to analyze data from the Alzheimer’s Disease Neuroimaging Initiative (ADNI). We illustrate the effects of covariates via our proposed tangent-normal decomposition. Our techniques shed fresh light on the neurological progression of Alzheimer’s disease. To maintain a specific emphasis in our study, we concentrate on examining the influence of the APOE-4 allele on brain anatomical structure. This analysis takes into account other covariates such as age, gender, and scores from the Mini-Mental State Examination (MMSE). We focus on fornix in this section.

To achieve this goal, the *typical* covariate vector is given as follows

$$\bar{\mathbf{X}}_T^{(g)} = [1, \bar{X}_{age}^{(g)}, \bar{X}_{T,gender} = 0, \bar{X}_{MMSE}^{(g)}, X_{T,APOE} = 0] \quad (8)$$

or

$$\bar{\mathbf{X}}_T^{(g)} = [1, \bar{X}_{age}^{(g)}, \bar{X}_{T,gender} = 1, \bar{X}_{MMSE}^{(g)}, X_{T,APOE} = 0] \quad (9)$$

where Equations (10) and (11) are the *typical* covariate vectors of male and female, respectively. We consider the wild type of APOE-4 (i.e., $X_{T,APOE} = 0$) as *typical*. The terms $\bar{X}_{age}^{(g)}$ and $\bar{X}_{MMSE}^{(g)}$ are the averages of age and MMSE within group g . We decompose the gender specification into male and female, in order to provide the gender-specific inference.

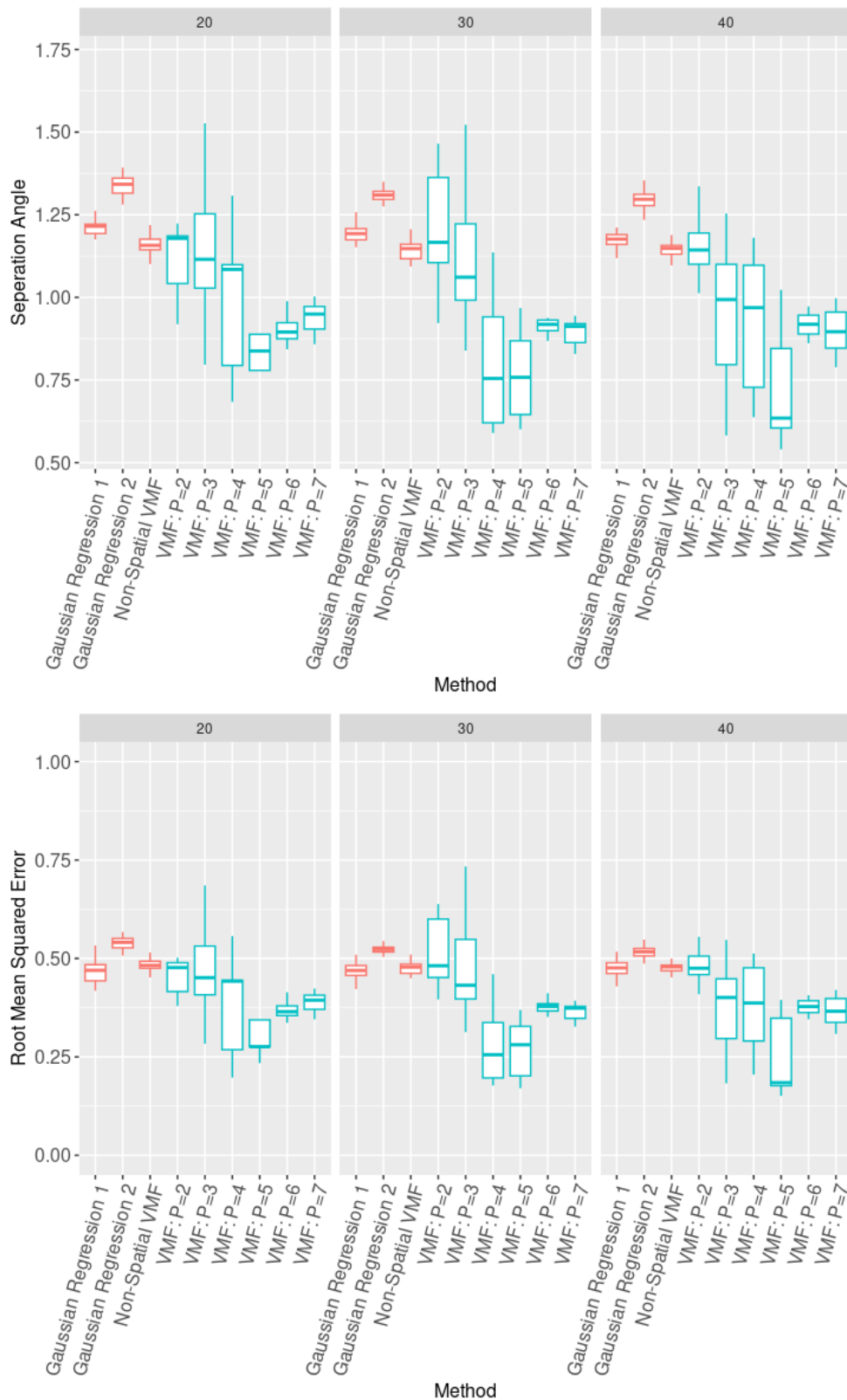


Figure 4: Comparison of Prediction errors quantified in terms of separation angles and root-mean-squared errors between the observed and predicted means. For the proposed vMF model, errors for different choices of spatial lags from 2 to 7 are provided.

The corresponding *specific* covariate vector is given as

$$\bar{\mathbf{X}}_S^{(g)} = [1, \bar{X}_{age}^{(g)}, \bar{X}_{T,gender} = 0, \bar{X}_{MMSE}^{(g)}, X_{S,APOE} = 1] \quad (10)$$

or

$$\bar{\mathbf{X}}_S^{(g)} = [1, \bar{X}_{age}^{(g)}, \bar{X}_{s,gender} = 1, \bar{X}_{MMSE}^{(g)}, X_{S,APOE} = 1], \quad (11)$$

where the APOE-4 status is considered as mutated (i.e., $X_{S,APOE} = 1$).

To incorporate group-level analysis into our study, we use the superscript (g) to denote group-specific terms. In this section, we focused on the investigation of the effect of APOE-4. The posterior $[m_v^{(g)}|\text{data}]$ implies the strength of the covariate effect and we consider $m_v^{(g)} > 0.65$ as large impact. Therefore, we calculate the posterior probabilities for $Pr(m_v^{(g)} - 0.65|\text{data})$. As an exploratory analysis, we consider the voxels whose posterior z-value larger than the 9-th quantile of the posterior z-values over voxels and group as *impacted* voxels. The visualization of the ADNI group is in Figure 5. Compared to other clinical groups (see Figure A.2 in supplementary materials), the ADNI group’s fornix anatomical structure is more impacted by the factor of APOE. Also, male has more laterality of the APOE effect, compared to women. Male’s left component of fornix is more impacted by the factor of APOE.

5 Conclusion and Discussion

This paper presents a novel spatial generalized linear regression framework for modeling spatially varying directional data as an outcome. The framework leverages a vMF-distributed error model, shown to accurately capture local, covariate-dependent variations. Given the directional nature of the data, we employ an autoregressive framework to capture spatial variations. Numerical evaluations, performed on both real and synthetic data, demonstrate our proposed method’s superior performance. By applying our pro-

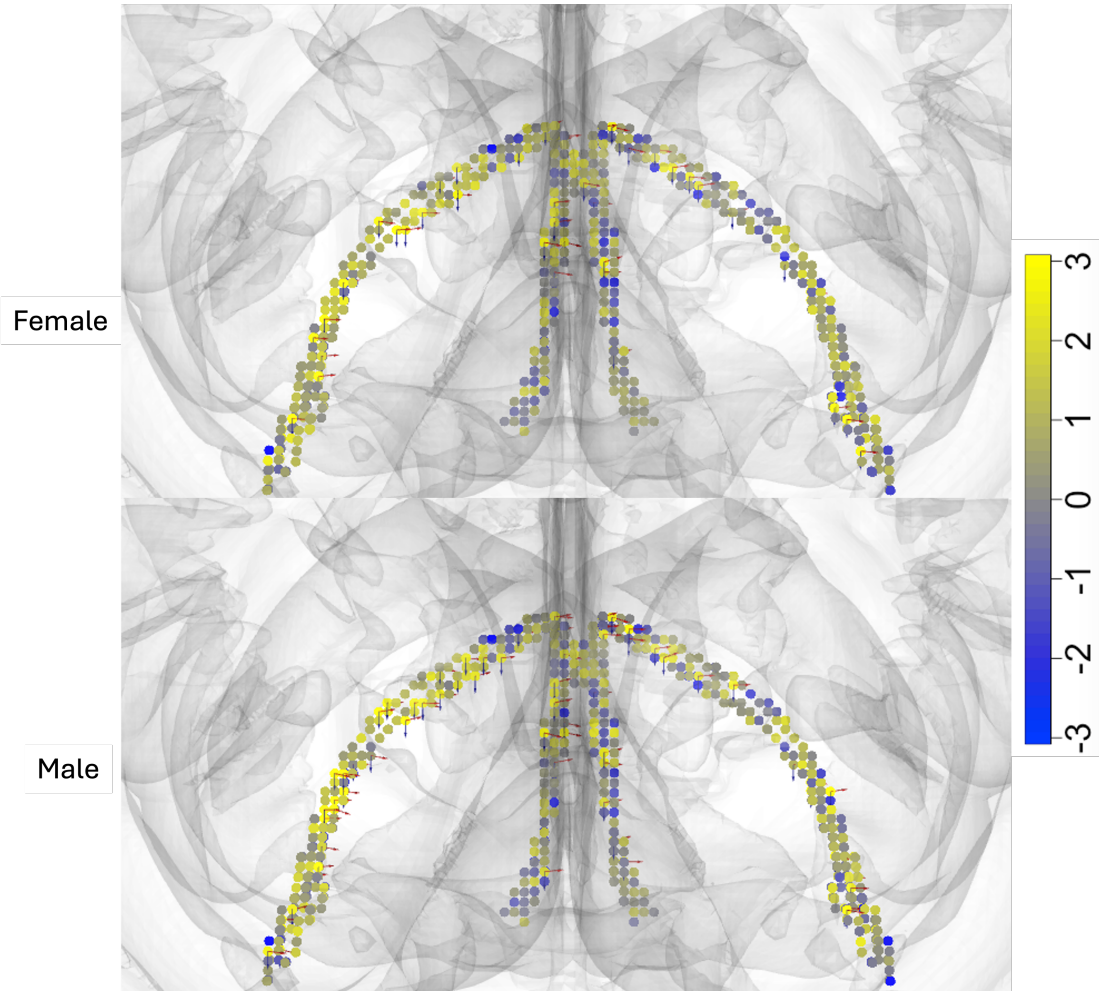


Figure 5: We present a tangent-normal decomposition of APOE-4 with a specific focus on the fornix as our region of interest. The upper panel is for female and the lower panel is for male. The colors are for the posterior z-scores. For *impacted* voxels, the red arrows are for *typical* mode directions and the blue arrows are for *specific* mode directions.

posed Bayesian angular inference scheme to the ADNI data, we have gleaned several novel scientific insights.

Our current analysis is cross-sectional. However, the exploration of longitudinal changes, specific to our ADNI study, akin to (Wang and Guo, 2019; Kundu et al., 2019), could be intriguing for identifying underlying mechanistic changes over time. Nonetheless, such covariate-dependent longitudinal research poses significant challenges. For instance, brain images and other biomarkers are often measured asynchronously (Li et al., 2022). In future work, extending our generalized vMF regression to accommodate asynchronously collected longitudinal data would be an interesting direction to pursue. Furthermore, our proposed model can be seamlessly integrated into other popular inference frameworks, such as mediation analysis, providing additional avenues of interest. In the context of analyzing DTI data, it will be interesting to incorporate fiber-shape information for more holistic analysis (Yeh, 2020). Future research will explore such a direction.

One of the most important aspects of our proposed model is the incorporation of spatial dependence. Thus, one may consider other modeling choices for the directional distribution and link functions proposed in the literature (Scealy and Welsh, 2017; Scealy and Wood, 2019; Paine et al., 2020) and integrate spatial dependence. The proposed autoregressive spatial dependence can still be applied under these other modeling choices seamlessly. It is thus an important future research avenue to compare these different modeling choices holistically for spatially dependent directional data. Another direction of future research is to consider a scale mixture of vMF distribution to characterize the data, which will allow different subjects to have different κ 's. Another generalization is possible in the specification of κ . We have now kept it fixed for all the spatial locations. It might be interesting to allow κ to vary slowly. Furthermore, unimodality might be a restrictive assumption.

References

- Aisen, P. S., Petersen, R. C., Donohue, M. C., Gamst, A., Raman, R., Thomas, R. G., Walter, S., Trojanowski, J. Q., Shaw, L. M. and Beckett, L. A. (2010), ‘Clinical core of the Alzheimer’s disease neuroimaging initiative: progress and plans’, Alzheimer’s & Dementia **6**(3), 239–246.
- Banerjee, S., Alaimo Di Loro, P., Mingione, M., Lipsitt, J., Batteate, C. and Jerrett, M. (2023), ‘Bayesian hierarchical modeling and analysis for actigraph data from wearable devices’.
- Barnett, G., Kohn, R. and Sheather, S. (1996), ‘Bayesian estimation of an autoregressive model using Markov chain Monte Carlo’, Journal of Econometrics **74**(2), 237–254.
- Cahn, A. J., Little, G., Beaulieu, C. and Tétreault, P. (2021), ‘Diffusion properties of the fornix assessed by deterministic tractography shows age, sex, volume, cognitive, hemispheric, and twin relationships in young adults from the human connectome project’, Brain Structure and Function **226**(2), 381–395.
- Chang, T. (1986), ‘Spherical regression’, The Annals of Statistics **14**(3), 907–924.
- Cornea, E., Zhu, H., Kim, P., Ibrahim, J. G. and Initiative, A. D. N. (2017), ‘Regression models on riemannian symmetric spaces’, Journal of the Royal Statistical Society: Series B (Statistical Methodology) **79**(2), 463–482.
- Downs, T. (2003), ‘Spherical regression’, Biometrika **90**(3), 655–668.
- Fisher, N. I. and Lee, A. J. (1992), ‘Regression models for an angular response’, Biometrics pp. 665–677.
- Goodlett, C. B., Fletcher, P. T., Gilmore, J. H. and Gerig, G. (2009), ‘Group analysis of DTI

- fiber tract statistics with application to neurodevelopment', Neuroimage **45**(1), S133–S142.
- Gould, A. L. (1969), 'A regression technique for angular variates', Biometrics pp. 683–700.
- Heidelberger, P. and Welch, P. D. (1981), 'A spectral method for confidence interval generation and run length control in simulations', Communications of the ACM **24**(4), 233–245.
- Hinkle, J., Fletcher, P. T. and Joshi, S. (2014), 'Intrinsic polynomials for regression on riemannian manifolds', Journal of Mathematical Imaging and Vision **50**, 32–52.
- Johnson, R. A. and Wehrly, T. E. (1978), 'Some angular-linear distributions and related regression models', Journal of the American Statistical Association **73**(363), 602–606.
- Kent, J., Mardia, K. and McDonnell, P. (2006), 'The complex bingham quartic distribution and shape analysis', Journal of the Royal Statistical Society Series B: Statistical Methodology **68**(5), 747–765.
- Kundu, S., Lukemire, J., Wang, Y. and Guo, Y. (2019), 'A novel joint brain network analysis using longitudinal Alzheimer's disease data', Scientific reports **9**(1), 1–18.
- Li, T., Li, T., Zhu, Z. and Zhu, H. (2022), 'Regression analysis of asynchronous longitudinal functional and scalar data', Journal of the American Statistical Association **117**(539), 1228–1242.
- Lindgren, F. and Rue, H. (2015), 'Bayesian spatial modelling with r-inla', Journal of statistical software **63**, 1–25.
- Mahan, R. P. (1991), Circular statistical methods: Applications in spatial and temporal performance analysis, Vol. 16, US Army Research Institute for the Behavioral and Social Sciences.

- Mardia, K. V. and Jupp, P. E. (2009), Directional statistics, Vol. 494, John Wiley & Sons.
- Murphy, E., Huang, W., Bessac, J., Wang, J. and Kotamarthi, R. (2022), ‘Joint modeling of wind speed and wind direction through a conditional approach’, arXiv preprint arXiv:2211.13612 .
- Neto, J. H. V., Schmidt, A. M. and Guttorp, P. (2014), ‘Accounting for spatially varying directional effects in spatial covariance structures’, Journal of the Royal Statistical Society: Series C: Applied Statistics pp. 103–122.
- Paine, P. J., Preston, S., Tsagris, M. and Wood, A. T. (2020), ‘Spherical regression models with general covariates and anisotropic errors’, Statistics and Computing **30**, 153–165.
- Pewsey, A. and García-Portugués, E. (2021), ‘Recent advances in directional statistics’, Test **30**(1), 1–58.
- Podcasy, J. L. and Epperson, C. N. (2022), ‘Considering sex and gender in Alzheimer disease and other dementias’, Dialogues in clinical neuroscience .
- Presnell, B., Morrison, S. P. and Littell, R. C. (1998), ‘Projected multivariate linear models for directional data’, Journal of the American Statistical Association **93**(443), 1068–1077.
- Rosenthal, M., Wu, W., Klassen, E. and Srivastava, A. (2014), ‘Spherical regression models using projective linear transformations’, Journal of the American Statistical Association **109**(508), 1615–1624.
- Sadigh-Eteghad, S., Talebi, M. and Farhoudi, M. (2012), ‘Association of apolipoprotein e epsilon 4 allele with sporadic late onset Alzheimer’s disease. a meta-analysis’, Neurosciences Journal **17**(4), 321–326.
- Scealy, J. and Welsh, A. (2017), ‘A directional mixed effects model for compositional expenditure data’, Journal of the American Statistical Association **112**(517), 24–36.

- Scealy, J. and Wood, A. T. (2019), ‘Scaled von mises–fisher distributions and regression models for paleomagnetic directional data’, Journal of the American Statistical Association .
- Schwartzman, A., Dougherty, R. F. and Taylor, J. E. (2005), ‘Cross-subject comparison of principal diffusion direction maps’, Magnetic Resonance in Medicine: An Official Journal of the International Society for Magnetic Resonance in Medicine **53**(6), 1423–1431.
- Schwartzman, A., Mascarenhas, W. F. and Taylor, J. E. (2008), ‘Inference for eigenvalues and eigenvectors of Gaussian symmetric matrices’, The Annals of Statistics **36**(6), 2886–2919.
- Soares, J. M., Marques, P., Alves, V. and Sousa, N. (2013), ‘A hitchhiker’s guide to diffusion tensor imaging’, Frontiers in neuroscience **7**.
- Straub, J. (2017), ‘Bayesian inference with the von-mises-fisher distribution in 3d’.
- Valdés Cabrera, D., Stobbe, R., Smyth, P., Giuliani, F., Emery, D. and Beaulieu, C. (2020), ‘Diffusion tensor imaging tractography reveals altered fornix in all diagnostic subtypes of multiple sclerosis’, Brain and behavior **10**(1), e01514.
- Wang, Y. and Guo, Y. (2019), ‘A hierarchical independent component analysis model for longitudinal neuroimaging studies’, NeuroImage **189**, 380–400.
- Yeatman, J. D., Dougherty, R. F., Myall, N. J., Wandell, B. A. and Feldman, H. M. (2012), ‘Tract profiles of white matter properties: automating fiber-tract quantification’, PloS one **7**(11), e49790.
- Yeh, F.-C. (2020), ‘Shape analysis of the human association pathways’, Neuroimage **223**, 117329.

Yeh, F.-C., Panesar, S., Fernandes, D., Meola, A., Yoshino, M., Fernandez-Miranda, J. C., Vettel, J. M. and Verstynen, T. (2018), ‘Population-averaged atlas of the macroscale human structural connectome and its network topology’, Neuroimage **178**, 57–68.

Zhu, H., Kong, L., Li, R., Styner, M., Gerig, G., Lin, W. and Gilmore, J. H. (2011), ‘FADTTS: functional analysis of diffusion tensor tract statistics’, NeuroImage **56**(3), 1412–1425.